Nuclear Materials and Energy 12 (2017) 148–155

Contents lists available at ScienceDirect

Nuclear Materials and Energy

journal homepage: www.elsevier.com/locate/nme

Transient heat load challenges for plasma-facing materials during long-term operation

M. Wirtz[a,*], J. Linke[a], Th. Loewenhoff[a], G. Pintsuk[a], I. Uytdenhouwen[b]

[a] Forschungszentrum Jülich GmbH, Institut für Energie- und Klimaforschung, Partner of the Trilateral Euregio Cluster (TEC), 52425 Jülich, Germany
[b] SCK•CEN, The Belgian Nuclear Research Centre, Boeretang 200, 2400 Mol, Belgium

ARTICLE INFO

Article history:
Received 21 July 2016
Revised 22 November 2016
Accepted 20 December 2016
Available online 27 December 2016

Keywords:
Tungsten
Edge localized mode
Transient thermal loads
Material degradation
High pulse numbers
Recrystallisation

ABSTRACT

The study summarizes the experimental results on fusion relevant pure heat load exposures of different tungsten products in the electron beam devices JUDITH 1 and 2. Besides steady state heat loading, up to 10^6 transient ELM-like pulses were applied. A detailed postmortem analysis reveals a wide and complex range of thermally-induced surface modifications and damages, such as roughening due to plastic deformation, cracking, and melting of parts of the material surface. Different industrially available tungsten products with varying thermal and mechanical properties were investigated in order to examine their influence on the thermal shock response. Furthermore, recrystallisation of the material, which will take place during long term operation, will additionally deteriorate the mechanical strength of the plasma facing material. The results show that the mechanical strength of the material has a significant influence on the formation and evolution of damage. Especially, recrystallisation and melting/resolidification will make the material more prone to thermal shock and fatigue, accelerating the evolution of damages. The combination of different material modifications/damages accompanied by the degradation of mechanical properties will have a strong impact on the plasma performance and lifetime of plasma facing materials/components.

1. Introduction

The use of plasma facing materials (PFM) over a long period of time (on the order of many years for the first ITER divertor) entails serious lifetime challenges. Tungsten, which will be used in the divertor region, will be exposed to severe and complex environmental conditions. Beside steady state heat loads of up to 20 MWm^{-2} and transient events with power densities up to 1 GWm^{-2} during normal operation, the PFMs also have to withstand high H, He and, although due to geometrical reasons partially shielded, neutron fluxes [1–3]. So called off-normal events, such as vertical displacement events (VDEs) and plasma disruptions, will deposit even higher power densities on the PFM [1–3]. Most of the current research directed towards material resilience does not consider long term effects like surface fatigue by high frequency transient thermal loads or morphology changes due to creep induced by (quasi-) stationary thermal loads [4–6]. The current status and available experimental results, as well as the issues that have been identified but not yet tackled, will be presented.

In the frame of previous studies the mechanical properties of various industrially produced tungsten products with different mechanical properties (especially the W-Ta alloys) were characterised and tested under fusion relevant thermal loads in the electron beam devices JUDITH 1 and 2 [7–9]. Special attention was paid to the grain orientation/microstructure, as well as to the recrystallised state of the materials which will have a significant influence on the material behaviour and its mechanical properties [10–12]. In order to investigate the dependence of the damage formation on the grain structure and mechanical strength, low pulse number tests on different tungsten products with different power densities and base temperatures were performed. High pulse number tests (up to 10^6 pulses) were applied on only one material but with different grain orientations, as well as in the recrystallised state, to investigate the fatigue and long term behaviour of the material. Additionally, tensile tests at different base temperatures and grain orientation were done. The obtained results reveal how the microstructure and mechanical properties are interconnected, and how that relationship affects the thermal shock response of tungsten as a PFM in a tokamak, like ITER or DEMO.

* Corresponding author.
E-mail address: m.wirtz@fz-juelich.de (M. Wirtz).

http://dx.doi.org/10.1016/j.nme.2016.12.024

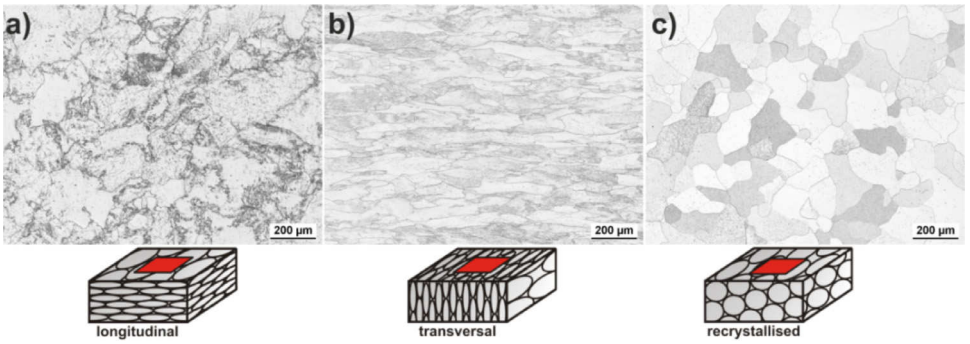

Fig. 1. Top view light microscope images of representative examples of the deformed microstructure after the forging process: a) perpendicular to the forging direction (L); b) parallel to the forging direction (T); c) in the recrystallised (R) state (1600 °C for 1 h). The area heated by electron beam is indicated by a red square. (For interpretation of the references to colour in this figure legend, the reader is referred to the web version of this article.)

2. Material properties and experimental conditions

Four tungsten products manufactured by Plansee SE, Austria were subject to microstructure analysis, tensile tests, and low pulse number experiments in JUDITH 1. These products are ultra-high purity tungsten (W-UHP, 99.9999 wt%), tungsten-vacuum-metallizing-tungsten (WVM, 15 – 40 ppm potassium) [13], and two tungsten tantalum alloys with 1 wt% (WTa1) and 5 wt% (WTa5) of tantalum, respectively. The materials were sintered into a rod shape, thermo-mechanically deformed in an axial direction to obtain a round blank, with a height of ~29 mm and a diameter of ~160 mm, and stress relieved at 1000 °C. Due to axial forging, the grains, were heavily deformed to a disc-like shape perpendicular to the forging direction as shown in Fig. 1a and b.

Parts of these materials were recrystallised (see Fig. 1c) according to the specifications of the supplier. W-UHP, WVMW and WTa1 were recrystallised at 1600 °C while WTa5 had to be heated to 1800 °C, because the high amount of tantalum increases the recrystallisation temperature. All four tungsten grades were kept at these temperatures for 1 h.

Based on differences in grain structure three different sample types were cut from each material. Longitudinal (L) with grains oriented parallel to the loaded surface/direction, transversal (T) with a perpendicular grain orientation, which is the preferred one for ITER, and recrystallised (R) (see Fig. 1 for schematic drawings). The elongation/deformation perpendicular to the forging direction is the same for all four tungsten products. After recrystallisation, the anisotropy of the grains nearly disappeared.

The major microstructural difference between the three tungsten grades is the grain size. W-UHP (average grain area ~4445 µm², aspect ratio L 0.8; T 0.3) grains are much larger than the grains of WVMW (average grain area ~533 µm², aspect ratio L 0.5; T 0.2), WTa1 (average grain area ~34 µm², aspect ratio L 0.5; T 0.3), or WTa5 (average grain area ~74 µm², aspect ratio L 0.7; T 0.2). The WTa materials have the smallest grains of all investigated materials. A possible explanation for the differences in grain size could be the addition of foreign atoms (potassium/tantalum).

Foreign atoms represent obstacles and accordingly limit grain growth during the manufacturing process. However, all materials show a more homogeneous grain structure and exhibit grain growth after above mentioned thermal treatment (see Fig. 1c) [14].

Tensile tests with a deformation rate of 0.2 mm/min (deformation rate 10^{-4} s^{-1}) were performed for all four tungsten products with L, T and R microstructure (see Fig. 1) at temperatures of 300 °C and 500 °C in a high temperature vacuum furnace set-up at SCK•CEN, Mol [15]. Fig. 2 shows the obtained engineering stress-strain curves.

Besides the expected decrease of the mechanical strength and increasing ductility at elevated temperatures for all L and R tungsten products [16,17,18], it can be stated that with an increasing amount of tantalum, the mechanical strength of the material increases. However, this improvement of tensile strength is accompanied by a significant reduction of the total elongation. Both effects can be explained by the solid solution hardening of tungsten obtained by adding tantalum in the matrix [17,18]. W-UHP exhibits the lowest tensile strength and fracture strain, which is caused by the much higher purity and the resulting lack of foreign atoms that also causes an increase of the DBTT (ductile-to-brittle-transition-temperature) [17,19]. In contrast to the L specimens, the T samples exhibit much lower mechanical strength and show brittle behaviour even at 500 °C. The reason for this anisotropic behaviour of material parameters is the so called texture strengthening effect [17,20]. For the R samples, the tensile strength is the lowest of all tested materials and grain orientations. However, the total elongation is significantly higher than for the L or T grain orientation. The changes of the material parameters after recrystallisation can be explained by the thermally-activated reduction in the defect density and the resulting poor cohesion between single grains [16].

The simulation of transient thermal shocks was done with the electron beam devices JUDITH 1 and 2 at Forschungszentrum Jülich.

2.1. JUDITH 1

For the low pulse number thermal shock tests in JUDITH 1, $12 \times 12 \times 5$ mm³ samples were cut from all four materials with L, T and R microstructure (see Fig. 1, bottom row). All samples were mechanically polished (SiC paper and diamond paste down to 0.25 µm) to a mirror finish to define an undamaged state with a surface roughness of approx. 0.1 µm. The samples were loaded with ELM relevant power densities between 0.19 GW/m² and 1.51 GW/m². These values were calculated by taking an electron absorption coefficient of 0.55 into account. A homogeneous loading of the samples was achieved by exposing a small area (4×4 mm²) with a focused electron beam (diameter of ~ 1 mm) at very high scanning frequencies (47 kHz in x-direction and 43 kHz in y-direction). All tests were performed with a pulse duration of 1 ms and a total number of 100 pulses. The inter-pulse time was ~ 3 s to allow a complete cool down. In addition to tests performed at room temperature (RT), a graphite holder with a tubular heating cartridge was used to achieve base temperatures up to 600 °C.

2.2. JUDITH 2

High pulse number tests were performed in the electron beam facility JUDITH 2 at Forschungszentrum Jülich. The test

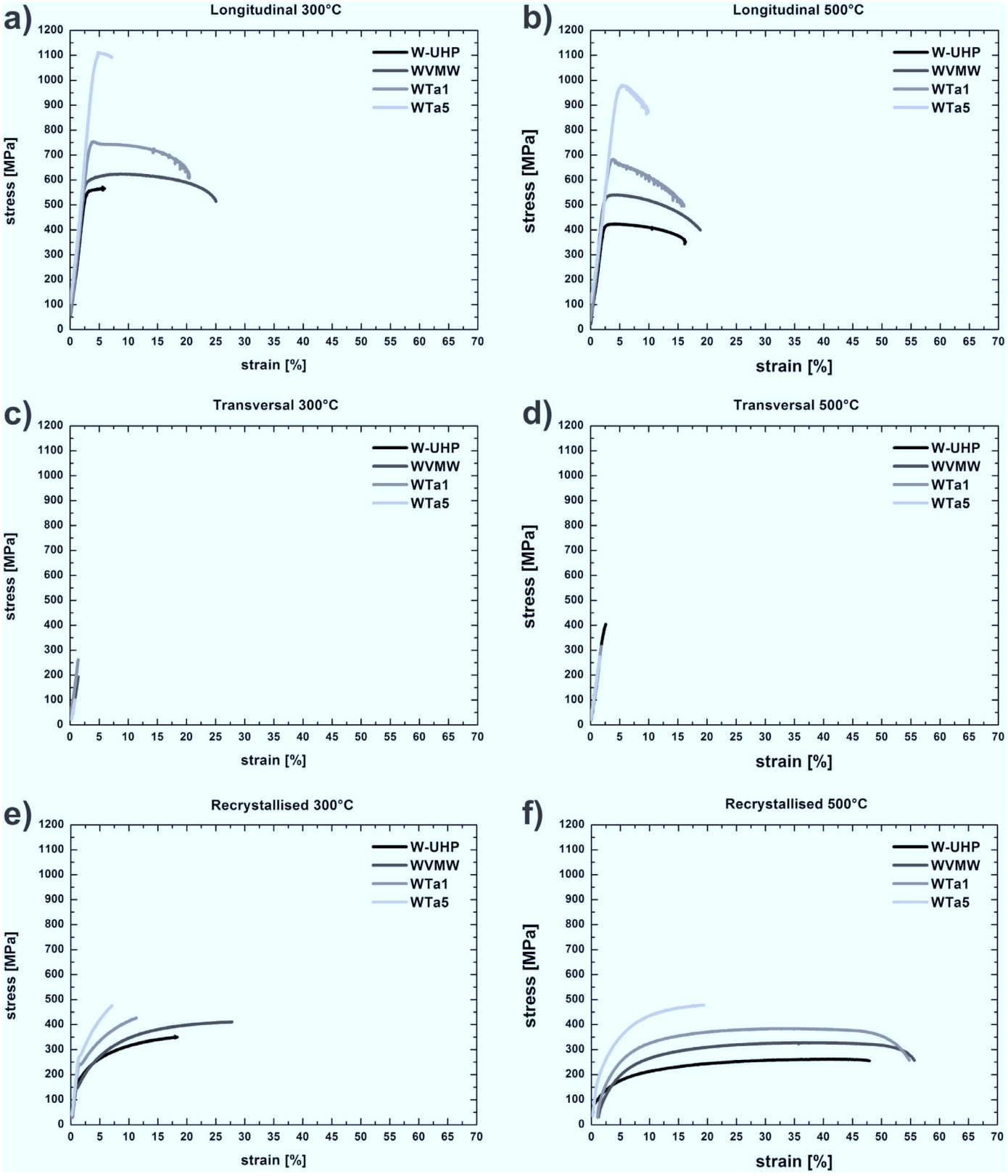

Fig. 2. Engineering stress-strain diagrams of W-UHP, WVMW, WTa1 and WTa5 with longitudinal (a + b) and transversal (c + d) grain orientation as well as in the recrystallised state (e + f) with a deformation speed of 0.2 mm/min at 300 °C and 500 °C.

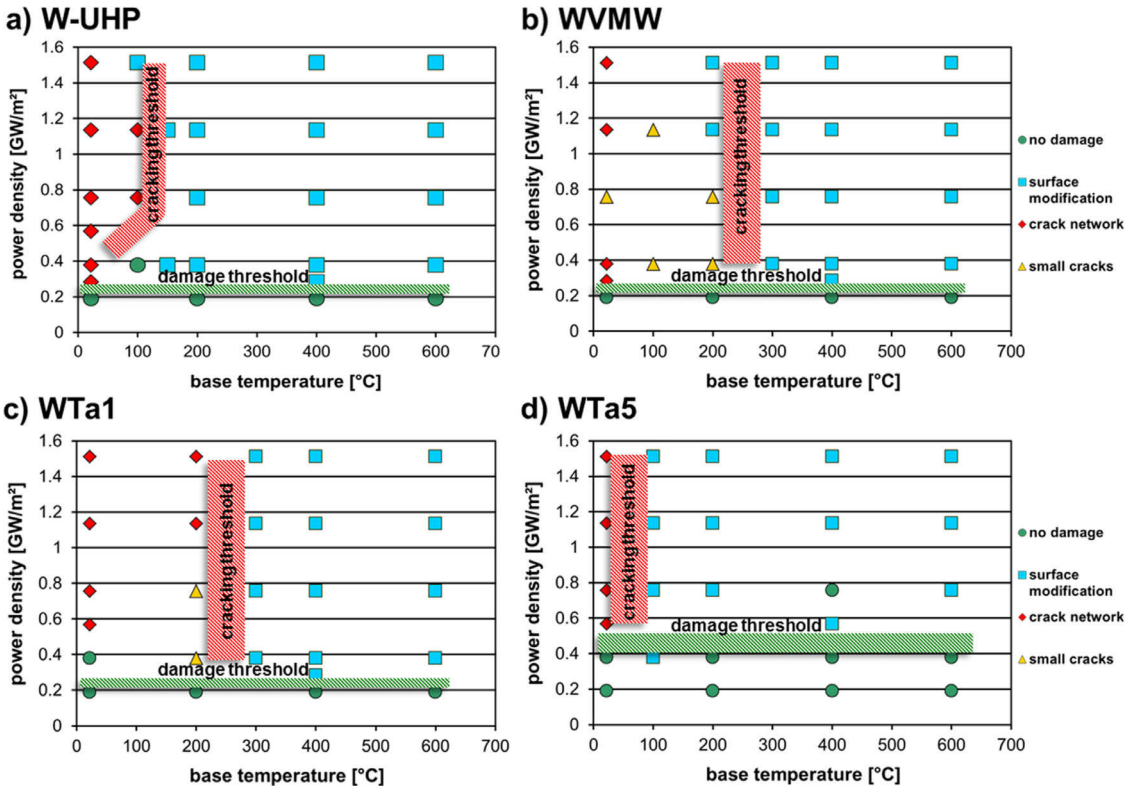

Fig. 3. Thermal shock damage mappings after 100 thermal shock events for (a) W-UHP, (b) WVMW, (c) WTa1 and (d) WTa5 with longitudinal (L) grain orientation [21,22].

components consisted of tungsten tiles measuring $12 \times 12 \times 5$ mm³ brazed to an actively-cooled copper block. The tiles were cut from the pure tungsten grade with L, T and R grain structure and polished to mirror-like finish. The thermal shock tests were performed with power densities ranging from 0.14 to 0.55 GW/m^2 (electron absorption coefficient of 0.55), a pulse duration of 0.48 ms, pulse numbers between 10^3–10^6 (loading frequency 25 Hz) and a SHL (stationary heat load) of 10 MW/m^2. As the cooling circuit is operated with 100 °C hot water and the transient pulses also heat up the sample, the resulting surface temperature (T_{surf}) immediately before the next transient pulse is 700 °C. All tests with $> 10^4$ pulses were interrupted every 10^4 pulses (i.e. after 400 s) for 20 s, allowing the component to return to its initial temperature (100 °C) and resembling a single ITER discharge.

After the exposure in JUDITH 1 and 2 the induced damages were investigated by SEM and laser profilometry. Subsequently, the cross sections of the samples were investigated by metallographic means to analyse the crack propagation into the bulk material.

3. Results and discussion

3.1. Low pulse number tests – JUDITH 1

Low pulse number tests (100 pulses) in JUDITH 1 were performed to compare the thermal shock behaviour of four different tungsten products in order to investigate which material parameters (mechanical strength, ductility and microstructure) influence the thermal shock damage response of tungsten. The obtained surface modifications and damages for all four materials with L grain orientation are depicted in Fig. 3. In these so called damage mappings the induced surface modifications and damages are colour and shape coded. This method of presentation helps to clearly define damage (no visible damage formation below a certain power density) and cracking (no crack formation above a certain base temperatures) thresholds for each material after 100 thermal shock events.

The comparison of the four different materials/damage mappings shows that there are significant differences in the damage response. One of the most interesting results is the location of the damage and cracking threshold of WTa5 L. The damage threshold is located between 0.4 GW/m² and 0.6 GW/m² and is roughly twice as high as that for the other three materials, for which the damage threshold is located at about 0.2 GW/m². Furthermore the cracking threshold for WTa5 L is located at a much lower temperature (between RT and 100 °C) than for the other materials where it varies between 100 °C and 150 °C for W-UHP L and between 200 °C and 300 °C for WVMW L and WTa1 L, respectively. An explanation for the difference in the damage behaviour can be found in Fig. 2a and b. The engineering stress-strain curves show clearly that the mechanical strength of WTa5 L is two times higher than that for the other materials, which is due to the solid solution hardening by tantalum as the other materials. For example, the yield strength of WTa5 L at 500 °C is 931 MPa while the yield strength for W-UHP L and WVMW L is 408 MPa and 513 MPa, respectively. WTa1 L has a value of 652 MPa which is also higher than that for W-UHP L and WVMW L but due to the lower tantalum content, not high enough to have a significant influence on the location of the threshold values. Admittedly, WTa 5 is not as ductile as the other materials due to the high content of foreign atoms but the significant increase of the mechanical strength seems to compensate this at least for low pulse numbers.

Based on the damage mappings for the L orientation (see Fig. 3), a reasonably reduced number of test parameters located around the damage threshold were chosen for further testing, because of the limited amount of samples/material. Fig. 4 shows damage mappings for WTa5 T and R, which are chosen as a representative example for the damage behaviour of these grain orientations and illustrate the superior performance of the L orientation.

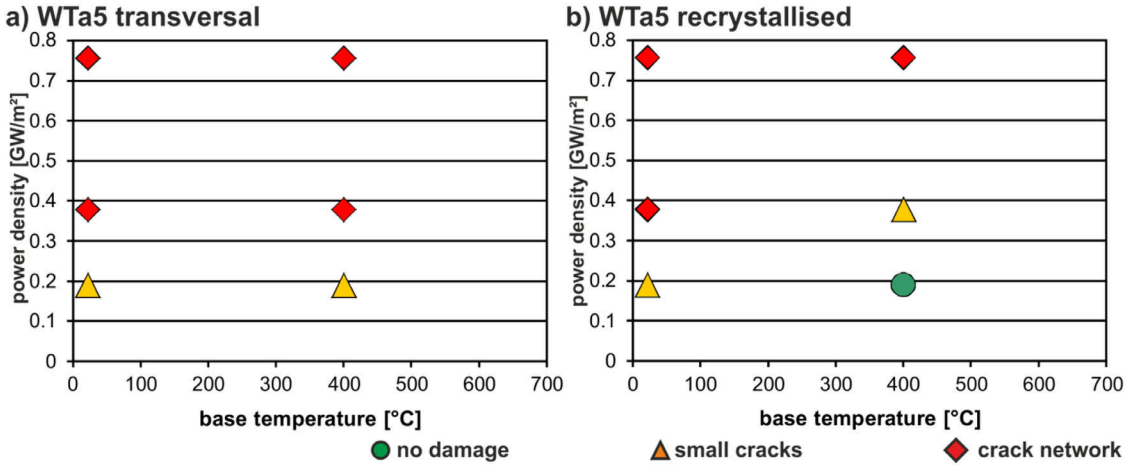

Fig. 4. Damage mapping of WTa5 with (a) transversal grain orientation and (b) in the recrystallised state.

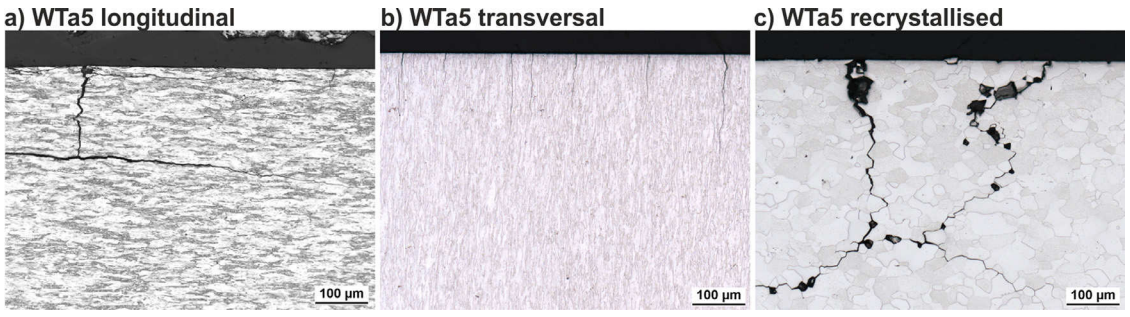

Fig. 5. Light microscope images of metallographic cross sections of WTa5 with (a) L, (b) T and (c) R grain orientation/structure exposed to 100 thermal shock events at RT with an absorbed power density of 0.76 GW/m².

Both T and R grain structures show a severe degradation in thermal shock performance. The damage threshold drops below 0.19 GW/m² (heat flux factor $F_{HF} \approx 6$ MW/m²s$^{0.5}$) and the cracking threshold increases to base temperatures above 400 °C. This degradation is caused by the significant drop of the mechanical strength for the T and R samples (roughly by a factor of two), as well as the brittle behaviour of tungsten with a transversal grain orientation, even at 500 °C (see Fig. 2c and d). As a result the damage evolution seems to be much faster for the T and R structures than for the L structures, and damages such as small cracks and thermal shock crack networks appear at lower power densities and higher base temperatures.

Beside the general investigation and classification of the induced thermal shock damages it is also of great importance to have a detailed look at the surface degradation due to thermal shock exposure. Fig. 5 gives representative examples of the thermal shock crack propagation in the material for different microstructures.

The crack propagation of the L (see Fig. 5a) and R (Fig. 5c) samples look very similar. They first propagate perpendicular to the loaded surface into the material, stop at a certain depth, and start to grow parallel to the surface. These parallel cracks act as a thermal barrier and cause overheating as well as melting of the surface and pose the risk to erode complete parts of the surface. Closer investigations show that for the L samples, the cracks propagate trans- and intergranular, while for the R samples, the cracks predominantly grow intergranular, which is a result of the poor cohesion between single grains [23]. This is also the reason for the grain loss during the preparation of the cross sections (see Fig. 5c) and the generally much larger crack depth in the recrystallised samples. These correlations between the crack propagation and the microstructure were found for all five tested tungsten products. The grain loss could become a major problem during long term operation. In contrast to L and R, the T samples show no cracking parallel to the loaded surface, and cracks propagate along the grain boundaries into the material. However, the crack densities are much higher due to the low mechanical strength and the brittle behaviour of the T sample. The abundance of surface cracks create a very dense network of leading edges on the surface which might become overheated and molten during long term operation in fusion devices and should be investigated in more detail in the future [24].

3.2. High pulse number tests – JUDITH 2

High pulse number tests were performed on pure tungsten (99.97 wt%) with different grain structures (L, T and R) which have similar mechanical properties compared to the pure tungsten material tested in Section 2, Fig. 2. The low pulse number tests have shown that thermal shock damages are induced for L samples at higher power densities than for the T and R samples due to their higher mechanical strength. Therefore, the high pulse number behaviour of the L samples was investigated first. Induced surface modifications and damages for the L samples are depicted in a damage mapping (see Fig. 6) with the same colour and shape coding as for the low pulse number tests. The only difference between the plots is that the X axis in Fig. 6 shows the number of applied thermal shock pulses and not the base temperature of the samples.

In contrast to the low pulse number tests discussed before, the high pulse number tests were performed at a fixed base temperature of 700 °C, and therefore the material is in a ductile regime (see Fig. 2) [8,9]. First, the damage threshold is lower (below 0.27 GW/m² or $F_{HF} \approx 6$ MW/m²s$^{0.5}$), than it was in the

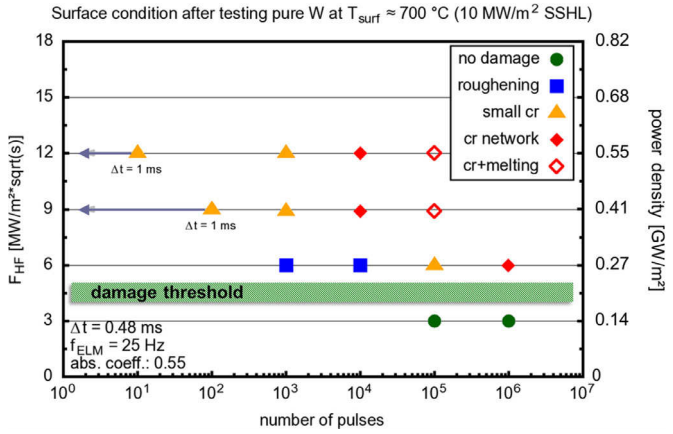

Fig. 6. Thermal shock damage mapping of pure tungsten with longitudinal grain orientation at a base temperature of 700 °C [26].

Table 1
Crack depth evolution of longitudinal tungsten samples with increasing number of pulses at a base temperature of 700 °C.

	10^3 pulses	10^4 pulses	10^5 pulses
0.41 GW/m²	10 ± 2 µm	53 ± 32 µm	162 ± 102 µm
0.55 GW/m²	21 ± 4 µm	63 ± 20 µm	218 ± 57 µm

low pulse number tests for the L samples (see Fig. 3, below $F_{HF} \approx 9$ MW/m²s$^{0.5}$). Above this threshold value, fatigue effects are clearly visible. At 0.27 GW/m², the tungsten surface shows roughening due to plastic deformation at up to 10^4 pulses. Further exposure induces small, arbitrarily distributed cracks which evolve into a thermal shock crack network after 10^6 pulses. The basic damage mechanism is the same for high and low pulse number tests.

During the thermal shock, the materials are subjected to thermal expansion, which is restricted by the colder surrounding material, generating compressive stresses. These stresses lead to plastic deformation if they overcome the yield strength of the material. After the thermal shock, the material shrinks during the cool down phase, but cannot return to its original state depending on the degree of plastic deformation, and the compressive stresses are converted into tensile stresses. Depending on the base temperature (below or above DBTT) these stresses can result in brittle cracks, which are formed during the first couple of pulses (see Figs. 3 and 4) or in fatigue cracks (see Figs. 6 and 8), respectively [25,26]. Fatigue cracks are caused by the weakening of a material by repeatedly applied loads and the accumulation of defects like dislocations. Once formed, these cracks constantly grow under further loading deeper into the material [25,27]. This fatigue crack growth is observed during the high pulse number tests, as is can be seen in Table 1. The cracks still grow deeper up to 10^5 thermal shock pulses in contrast to the brittle crack formation observed during the low pulse number test which are formed during the first 10 pulses and do not change in crack depth during further loading. It is likely that the cracks stop in a certain depth where the thermal gradients/stresses are insufficient to drive the crack deeper into the material. If the fatigue crack depth saturates or continuously grows with increasing number of pulses cannot be answered based on these results.

Besides the damage categories that have already been defined during the low pulse number tests, a new category, cracking plus melting, was found for the high pulse number tests. A representative example for this new damage category is shown in Fig. 7. In addition to the strong plastic deformation and cracking, small droplets of molten material are visible on the loaded surface, although the surface temperature on a pristine surface (base temperature plus temperature rise during the thermal shock of 0.41 GW/m² is ~ 1200 °C and for 0.55 GW/m² ~ 1400 °C) is not high enough to melt tungsten (see Fig. 7a). The explanation for this is that due to the severe plastic deformation and cracking, small parts of the materials lose contact with the bulk material. This causes a significant drop of the heat dissipation and results in overheating and melting of these structures. The loose contact of these structures to the bulk also poses the risk of enhanced erosion.

Metallographic cross sections of these structures (see Fig. 7b) show that the fatigue cracks tend to propagate not only perpendicular, but also parallel to the loaded surface, which causes overheating of the surface. As a result, the material starts to recrystallise in the near-surface region, even though the base temperature is below the recrystallisation temperature. Only the additional temperature rise during the thermal shock heats the material above the recrystallisation temperature. Tensile test results (see Fig. 2), in combination with the low pulse number tests (see Fig. 4b), show that recrystallisation has a significant influence on the mechanical properties of the materials and could increase the damage evolution significantly even if the pristine materials had much higher mechanical strength.

Similar to the low pulse number tests, the T and R microstructures were also exposed to high pulse number tests. The results are shown in Fig. 8. In contrast to the L samples the damage threshold drops below 0.14 GW/m² ($F_{HF} \approx 3$ MW/m²s$^{0.5}$) for the T and R samples, which mirrors the surface response during low pulse number tests. Furthermore, the formation of cracks starts at a lower number of pulses, i.e. small cracks are already formed after 10^4 pulses at 0.27 GW/m². Furthermore, the crack depth increases with increasing power density and number of pulses like the L samples (see Table 1). Similar to the low pulse number tests, the reason for this degradation of the thermal shock performance is due to the reduced mechanical strength of the T and R structures compared to the L orientation. Accordingly, damage evolution for T and R is much faster than for the L orientation [10,11,25,26].

4. Summary & conclusions

The obtained results show that the applied thermal shock loads induce a wide range of surface modifications and damages, which are strongly influenced by the material properties and microstructure. Low pulse number damage mappings of different tungsten products, with different mechanical and microstructural properties, have shown that yield/tensile strength as well as ductility, have a significant influence on the damage behaviour. The transversal grain orientation, which is the preferred one for ITER to prevent the formation of cracks parallel to the loaded surface, shows brittle behaviour even at elevated temperatures while recrystallised materials have a reduced mechanical strength. These changes in microstructure and materials properties lead to a significant drop in the damage threshold. Meanwhile, the solid solution hardening caused by adding tantalum increases the mechanical strength of the tungsten material, as well as the damage threshold, at the expense of a significant reduction of ductility.

High pulse number tests of pure tungsten with longitudinal and transversal grain orientation, as well as in the recrystallised state, support this finding. The results clearly indicate that roughening due to plastic deformation is a precursor for fatigue crack formation. Transversal and recrystallised specimens show thermal shock damage formation even at power densities below 0.14 GW/m² ($F_{HF} \approx 3$ MW/m²s$^{0.5}$) after 10^5 pulses. This is very low compare to the expected loading conditions in future fusion devices [1]. Therefore, further studies need to focus on the impact of such thermal shock and fatigue damages on the plasma performance like testing pre-damaged (fatigue and molten) components in a tokamak environment.

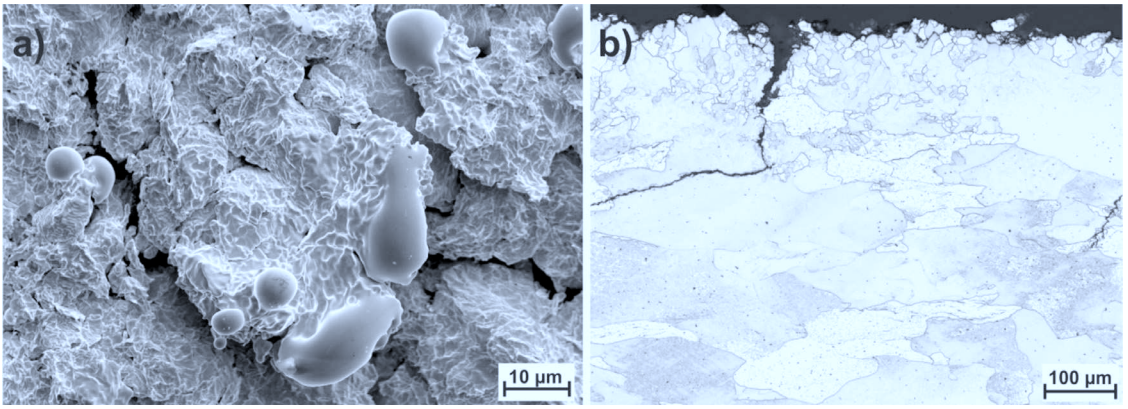

Fig. 7. New damage category cracking plus melting after 10^5 pules with 0.41 GW/m² at 700 °C: (a) SEM image of the surface; (b) light microscope image of the cross section.

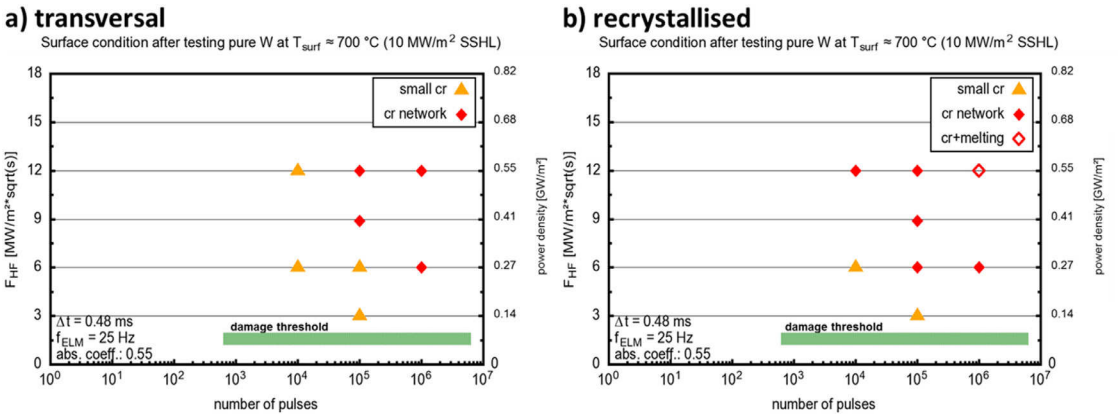

Fig. 8. Thermal shock damage mapping of pure tungsten with (a) transversal and (b) recrystallised grain structure at a base temperature of 700 °C.

Detailed post-mortem analyses of the induced damages showed critical crack formation parallel to the loaded surface for the longitudinal and recrystallised samples, which act as a thermal barrier and cause overheating, recrystallisation, and melting of near surface regions. Enhanced erosion of near surface grains is very likely for tungsten materials in the recrystallised state. Loss of material could contaminate the plasma, and in the worst case cause a breakdown of the fusion reaction. Due to the reduced mechanical strength of the recrystallised materials, damage evolution is much faster and might lead to an earlier failure of a plasma facing component. This leads to the assumption that the operation temperature of the divertor (stationary and transient heat loads) should stay below the recrystallisation temperature [1,17,28]. Furthermore, other investigations like [29] show that molten and re-solidified tungsten surfaces show very similar damage behaviour to recrystallised materials. Future studies therefore need to determine whether melting poses similar risks as recrystallisation does.

Besides just the pure thermal exposure of tungsten, high flux particle loading needs to be taken into account. H and He irradiation will change the mechanical and thermal properties of tungsten and hence have an influence on the thermal shock damage response. Due to H/He embrittlement, critical stresses for damage/cracking formation will be lower and also lead to faster damage evolution [30,31]. He-induced bubble formation directly below the surface reduces the thermal conductivity, and could lead to higher surface temperatures. In addition W-fuzz growth could lead to enhanced erosion of tungsten material [32,33]. Unfortunately, the impact of high energy neutrons on the performance of tungsten under transient heat loads, especially for high pulse number tests and simultaneous particle exposure, is not clear yet [34].

The combination of this wide range of environmental conditions makes the evaluation of tungsten and the prediction of possible damages and life-time very difficult and complex. However, it can be assumed that recrystallisation and molten/re-solidified surface structures have a detrimental influence on the lifetime of PFM and components. Therefore, further investigations of tungsten as PFM for long term operation with high accumulated neutron doses and the study of the influence of pre-damaged surfaces on the plasma performance in existing tokamaks are at the moment the important issues to be addressed for future fusion reactors.

Acknowledgment

This work has partially been carried out within the framework of the EUROfusion Consortium and has received funding from the Euratom research and training programme 2014–2018 under grant agreement No. 633053. The views and opinions expressed herein do not necessarily reflect those of the European Commission.

References

[1] R.A. Pitts, S. Carpentier, F. Escourbiac, T. Hirai, V. Komarov, S. Lisgo, A.S. Kukushkin, A. Loarte, M. Merola, A. Sashala Naik, R. Mitteau, M. Sugihara, B. Bazylev, P.C. Stangeby, J. Nucl. Mater. 438 (2013) S48–S56.
[2] M. Merola, D. Loesser, A. Martin, P. Chappuis, R. Mitteau, V. Komarov, et al., Fusion Eng. Des. 85 (2010) 2312–2322.
[3] A. Loarte, G. Saibene, R. Sartori, V. Riccardo, P. Andrew, J. Paley, W. Fundamenski, T. Eich, A. Herrmann, G. Pautasso, A. Kirk, G. Counsell, G. Federici, G. Strohmayer, D. Whyte, A. Leonard, R.A. Pitts, I. Landman, B. Bazylev, S. Pestchanyi, Phys. Scr. (2007) 222–228.
[4] T. Hirai, G. Pintsuk, J. Linke, M. Batilliot, J. Nucl. Mater. 390-391 (2009) 751–754.
[5] A. Suslova, O. El-Atwani, S. Harilal, A. Hassanein, Material ejection and surface morphology changes during transient heat loading of tungsten as plasma-facing component in fusion devices, Nucl. Fusion 55 (2015) 033007.

[6] Bardin, et al., J. Nucl. Mater. 463 (2015) 193–197 2015.
[7] R Duwe, W Kuehnlein, H Muenstermann, The new electron beam facility for materials testing in hot cells, Fusion Technol. (1994) 356–358.
[8] A. Schmidt, A. Bürger, K. Dominiczak, S. Keusemann, Th. Loewenhoff, J. Linke, et al., High heat flux testing of components for future fusion devices by means of the facility JUDITH 2„ in: International Conference on High-Power Electron Beam Technology (EBEAM 2010), Reno (USA), 2010, p. 571. ISBN 9781617823992.
[9] P. Majerus, R. Duwe, T. Hirai, W. Kühnlein, J. Linke, M. Rödig, Fusion Eng. Des. 75–79 (2005) 365–369.
[10] I. Steudel, A. Huber, J. Linke, G. Sergienko, B. Unterberg, M. Wirtz, Sequential and simultaneos thermal and particle exposure of tungsten, Phys. Scr. T167 (2016) art. no. 014053.
[11] M. Wirtz, G. Cempura, J. Linke, G. Pintsuk, I. Uytdenhouwen, Thermal shock response of deformed and recrystallised tungsten, Fusion Eng. Des. 88 (2013) 1768–1772.
[12] G. Pintsuk, A. Prokhodtseva, I. Uytdenhouwen, Thermal shock characterization of tungsten deformed in two orthogonal directions, J. Nucl. Mater. 417 (2011) 481–486.
[13] Plansee SE https://www.plansee.com/en/materials/tungsten.html (10.11.2016)
[14] W. Martienssen, H. Warlimont, Springer Handbook of Condensed Matter and Materials Data, Springer, Berlin, 2005 1120.
[15] I. Uytdenhouwen, Degradation of First Wall Materials under ITER Relevant Loading Conditions Ph.D thesis, University Ghent, 2010.
[16] W. Martienssen, H. Warlimont, Springer Handbook of Condensed Matter and Materials Data, Springer, Berlin, 2005.
[17] E. Lassner, W.-D. Schubert, Tungsten: Properties, Chemistry, Technology of the Element, Alloys, and Chemical Compounds, Kluwer Academic/Plenum Publishers, New York, 1999.
[18] E. Pink, R. Eck, Refractory Metals and their Alloys, Wiley-VCH Verlag GmbH & Co. KGaA, 2006.
[19] J.P. Morniroli, Low Temperature Embrittlement of Undoped and Doped Tungsten, Elsevire, London, 1989.
[20] G.L. Krask, Effect of impurities on the electronic structure of grain boundaries and intergranular cohesion in iron and tungsten, Mater. Sci. Eng. 234–236 (0) (1997) 1071–1074.
[21] J. Linke, Th. Loewenhoff, V. Massaut, G. Pintsuk, G. Ritz, M. Rödig, A. Schmidt, C. Thomser, I. Uytdenhouwen, V. Vasechko, M. Wirtz, Performance of different tungsten grades under transient thermal loads, Nucl. Fusion 51 (7) (2011) art. no. 073017.
[22] M. Wirtz, J. Linke, G. Pintsuk, L. Singheiser, I. Uytdenhouwen, Phys. Scr. T145 (2011) 4 014058, doi:10.1088/0031-8949/2011/T145/014058.
[23] F.J. Humphreys, M. Hatherly, Recrystallization and Related Annealing Phenomena, 2nd edition, Pergamon, 2003.
[24] A. Zhitlukhin, N. Klimov, I. Landman, J. Linke, A. Loarte, M. Merola, V. Podkovyrov, G. Federici, B. Bazylev, S. Pestchanyi, V. Safronov, T. Hirai, V. Maynashev, V. Levashov, A. Muzichenko, J. Nucl. Mater. 363–365 (2007) 301–307 15 June.
[25] Th. Loewenhoff, J. Linke, G. Pintsuk, C. Thomser, Tungsten and CFC degradation under combined high cycle transient and steady state heat loads, Fusion Eng. Des. 87 (2012) 1201–1205 with permission from Elsevier.
[26] G. Pintsuk, A. Prokhodtseva, I. Uytdenhouwen, Thermal shock characterization of tungsten deformed in two orthogonal directions, J. Nucl. Mater. 417 (2011) 481–486.
[27] A. Weronski, T. Hejwowski, Thermal Fatigue in Metals, Taylor & Francis, New York, 1991.
[28] V. Philipps, Tungsten as material for plasma-facing components in fusion devices, J. Nucl. Mater. 415 (2011) S2–S9.
[29] Th. Loewenhoff, J. Linke, J. Matejicek, M. Rasinski, M. Vostrak, M. Wirtz, Nucl. Mater. Energy (2016) in Press, doi:10.1016/j.nme.2016.04.004.
[30] M. Wirtz, S. Bardin, A. Huber, A. Kreter, J. Linke, T.W. Morgan, G. Pintsuk, M. Reinhart, G. Sergienko, I. Steudel, G. De Temmerman, B. Unterberg, Nucl. Fusion 55 (2015) 123017.
[31] G.G. van Eden, T. Morgan, H. van der Meiden, J. Matejicek, T. Chraska, M. Wirtz, G. De Temmerman, Nucl. Fusion 54 (12) (2014) art. no. 123010.
[32] S. Kajita, G.D. Temmerman, T. Morgan, S. van Eden, T. de Kruif, N. Ohno, Thermal response of nanostructured tungsten, Nucl. Fusion 54 (2014) 033005.
[33] D. Nishijima, R.P. Doerner, D. Iwamoto, Y. Kikuchi, M. Miyamoto, M. Nagata, I. Sakuma, K. Shoda, Y. Ueda, J. Nucl. Mater. 434 (2013) 230–234.
[34] G. Pintsuk, J. Compan, T. Hirai, J. Linke, M. Rödig, I. Uytdenhouwen, in: 2007 IEEE 22nd Symposium on Fusion Engineering, NM, Albuquerque, 2007, pp. 1–4, doi:10.1109/FUSION.2007.4337887.